Nebulised Gadolinium-Based Nanoparticles for a Multimodal Approach: Quantitative and Qualitative Lung Distribution Using Magnetic Resonance and Scintigraphy Imaging in Isolated Ventilated Porcine Lungs

Yoann Montigaud, Jérémie Pourchez, Lara Leclerc, Olivier Tillement, Anthony Clotagatide, Clémence Bal, Noël Pinaud, Nobuyasu Ichinose, Bei Zhang, Sophie Perinel, et al.

International Journal of Nanomedicine

Dovepress
open access to scientific and medical research

Open Access Full Text Article

ORIGINAL RESEARCH

Nebulised Gadolinium-Based Nanoparticles for a Multimodal Approach: Quantitative and Qualitative Lung Distribution Using Magnetic Resonance and Scintigraphy Imaging in Isolated Ventilated Porcine Lungs

This article was published in the following Dove Press journal:
International Journal of Nanomedicine

Yoann Montigaud[1]
Jérémie Pourchez[1]
Lara Leclerc[1]
Olivier Tillement[2]
Anthony Clotagatide[3,4]
Clémence Bal[5]
Noël Pinaud[5]
Nobuyasu Ichinose[6]
Bei Zhang[7]
Sophie Perinel[3,4]
François Lux[2,8]
Yannick Crémillieux[5]
Nathalie Prevot[3,4]

[1]Mines Saint-Etienne, Univ Lyon, Univ Jean Monnet, INSERM, U 1059 Sainbiose, Centre CIS, Saint-Etienne, France; [2]Institut Lumière Matière, Université de Lyon, Villeurbanne, France; [3]INSERM U 1059 Sainbiose, Université Jean Monnet, Saint-Etienne, France; [4]CHU Saint-Etienne, Saint-Etienne, France; [5]IBIO, Bordeaux, France; [6]Canon Medical Systems Corporation, Otawara, Japan; [7]Canon Medical Systems Europe, Zoetermeer, Netherlands; [8]Institut Universitaire de France (IUF), Paris, France

Correspondence: Jérémie Pourchez
Mines Saint-Etienne, 158 Cours Fauriel, CS 62362, Saint-Etienne, Cedex 2 42023, France
Tel +33 4 77 42 01 80
Email pourchez@emse.fr

Purpose: This study aims at determining lung distribution of gadolinium-based polysiloxane nanoparticles, AGuIX® (small rigid platform – SRP), as a potential theranostic approach by the pulmonary route.

Methods: First, the aerodynamic size distribution and the aerosol output rate were thoroughly characterized. Then, a multimodal approach using magnetic resonance (MR) and gamma-camera (GC) imaging allows to assess the deposition of the aerosolised nanoparticles in the respiratory tract using isolated ventilated porcine lungs.

Results: The SRP has proven to be radiolabelled by radioisotope with a good yield. Crude SRP or radiolabelled ones showed the same aerodynamic size distribution and output as a conventional molecular tracer, as sodium fluoride. With MR and GC imaging approaches, the nebulised dose represented about 50% of the initial dose of nanoparticles placed in the nebuliser. Results expressed as proportions of the deposited aerosol showed approximately a regional aerosol deposition of 50% of the deposited dose in the lungs and 50% in the upper airways. Each technique assessed a homogeneous pattern of deposited nanoparticles in Lungs. MR observed a strong signal enhancement with the SRP, similar to the one obtained with a commonly used MRI contrast agent, gadoterate meglumine.

Conclusion: As a known theranostic approach by intravenous administration, SRP appeared to be easily aerosolised with a conventional nebuliser. The present work proves that pulmonary administration of SRP is feasible in a human-like model and allows multimodal imaging with MR and GC imaging. This work presents the proof of concept of SRP nebulisation and aims to generate preclinical data for the potential clinical transfer of SRP for pulmonary delivery.

Keywords: aerosol, pulmonary delivery, ex vivo model, MRI, SPECT/CT, theranostic

Introduction

Since decades, nanoparticulate forms are developed to overcome the limitations of drugs by decreasing their intrinsic toxicities and/or by improving their efficacy. Therefore, many nanoparticles were preclinically tested and showed promising results on various therapeutic areas with an unmet medical need such as oncology, orphan diseases, infectiology, etc. However, almost all failed to be transposed in clinical trials

submit your manuscript | www.dovepress.com
DovePress
http://doi.org/10.2147/IJN.S260640

due to an overestimated efficacy, an unfavourable toxicological profile or difficulties concerning the scalability of the manufacturing process.

Among the few nanoparticulate forms that have been successfully translated to the clinics, the small rigid platform AGuIX® nanoparticles (SRP, NH Theraguix®, Villeurbanne, France) act as radiosensitizer and as MRI positive contrast agent.[1–4] These inorganic nanoparticles are composed of a polysiloxane matrix grafted with DOTAGA moieties mostly chelated by gadolinium, while a small fraction of these moieties – about 2% – remain free to chelate radioactive isotopes allowing multimodal imaging and, therefore, theranostic approach.[5–10]

SRP is currently implicated in two Phase II clinical trials on brain metastases (NANO-RAD2, NCT03818386 and NANO-STEREO: NCT04094077) and one phase Ib clinical trial on advanced cervical cancer (NANO-COL, NCT03308604).

Although being developed for intravenous administration (IV), pulmonary administration using either intratracheal instillation or nebulised aerosols is an approach that has been previously evaluated in mice.[11] Indeed, when administered by the pulmonary route, these nanoparticles can be used to generate specific contrast mechanisms in the lungs.

For pulmonary delivery, the size range of SRP – around 5 nm – is not large enough to ensure retention in the deep lung. Actually, most of them would be exhaled or deposited in the upper airways. It is commonly stated that the most adapted airborne particle sizes for lung targeting are between 2 and 5 μm[12]. Consequently, delivery of nanoparticles to the respiratory tract could be accomplished:

(i) by nebulisation of nanosuspensions[13–19] (i.e. generating airborne micron-size droplets containing nanoparticles using a nebuliser)
(ii) by aerosolisation of solid microparticles containing nanoparticles[20–23] (e.g. the Trojan horse concept based on the encapsulation of the nanocarriers into airborne microparticles).

Doubtless, the simplest way to administrate these nanoparticles to the lungs is to nebulise them as a suspension. In the present study, no pharmaceutical development was needed to generate a proof of concept. However, such development could be required to improve the stability of the suspension or to increase the efficiency of the nebulisation.

However, some challenges remain to be addressed to choose the most adapted nebulisation system (*e.g.* air-jet vs vibrating mesh technologies) according to the physicochemical features of the nanosuspension (viscosity, surface tension, etc.). The main challenge is to generate an aerosol of intact nanoparticles – no chemical or size changes – with appropriate aerodynamic performance to reach a relevant aerosol deposition in terms of dose and regional lung targeting. Indeed, the nebulisation technology could have a strong impact on aerosol features: modification of airborne droplet size, decreased aerosol output, enhanced nanoparticle aggregation within droplets or modified nanoparticle shape. For instance, many papers reported that jet nebulisation is generally more disruptive compared to vibrating-mesh nebulisation, for liposomes or polymeric nanoparticles.[13–19] Nevertheless, due to their physicochemical properties the SRP demonstrated a high stability,[6] being much less fragile than liposomes or polymeric nanoparticles, which made them promising candidates for jet nebulisation.

Within the framework of a potential clinical translation of nebulised SRP to treat lung diseases, the main objective of this work was to propose the proof of concept that SRP could be suitable for inhalation in a human-like lung model thanks to a conventional clinically used jet nebuliser. On the one hand, nebulisation performances (in terms of aerodynamic size, airborne nanoparticles output rate, etc.) were characterized in vitro using a cascade impactor according to the European standard procedure (NF EN 13544–1) for aerosol medical devices. On the other hand, quantitative and qualitative distribution of nebulised SRP were assessed in an ex vivo respiratory model by a multimodal approach (MRI and scintigraphic imaging). To determine if the SRP suspension induces modifications of nebulisation performances or in the regional aerosol deposition profile, comparison of molecular tracers with SRP nanotracers, either crude or radiolabelled with ^{111}In, were performed. Reference nebulisation performances were assessed with sodium fluoride (NaF) while regional aerosol deposition was assessed with gamma camera and magnetic resonance imaging with ^{99m} technetium diethylene triamine pentaacetic acid (9mTc-DTPA) or gadoterate meglumine, respectively.

Materials and Methods

Ex vivo Respiratory Model for Preclinical Aerosol Studies

The ex vivo respiratory model was composed of a human replica of upper airways connected to porcine lungs. This

original model was previously characterized and validated for preclinical regional aerosol studies[24,25] The Ear-Nose-Throat (ENT) replica, including laryngeal structures, was reconstructed from CT scans of a healthy adult subject and manufactured by 3D-printing technology. The scans were provided by the University Hospital of Saint-Etienne. Before radiological examination, patients received an explicit note informing them that their data could be used for research. Afterwards, a written and informed consent is given by patients. This use of patients' data was performed under the supervision of the Ethics Committee of Saint-Etienne hospital. This ENT replica was assessed by endoscopy and CT scans and then validated by a senior radiologist. It was previously used for nasal and pulmonary assessment of aerosol deposition.[24–28] Porcine respiratory tracts were kindly supplied by a slaughterhouse (DespiViandes, La Talaudière France) and passed all quality controls requested by French regulation. Visual controls of wounds and sutures were achieved, and a bronchoscopy was performed to ensure the absence of significant obstruction of proximal bronchi. Lungs were placed in a sealed enclosure and ventilated using a depression generator (SuperDimension®, Covidien, Dusseldorf, Germany). Mean depression inside the enclosure was −9 kPa (−92 cmH_2O). These relatively high negative pressures were two time the expected values, according to West.[29] Lungs were not used for more than 8 hours. The model was set in supine position with following breathing pattern: 15 cycles per minutes, tidal volume about 500 mL and dynamic compliance about 90 cmH_2O/mL as previously described.[26,30] A scheme of the model and complete description are provided in Supplementary Information.

Aerosol Medical Device

The chosen medical device was a PARI LC SPRINT (PARI GmbH, Starnberg, Germany) jet nebuliser, with a corresponding compressor PARI TurboBOY® SX (PARI GmbH, Starnberg, Germany).

Unless otherwise specified, the reservoir of the nebuliser was always filled with 3 mL of solution/suspension. Nebulisation was conducted until complete atomisation of the suspension.

Particle Aerodynamic Size Distribution

For all tracers (NaF, ^{99m}Tc-DTPA and SRP), the assessment of the mass median aerodynamic diameter (MMAD) was performed in triplicate using a 12-stage DLPI cascade impactor (Dekati Low Pressure Impactor, Dekati Ltd., Kangasala, Finland) operated at an airflow of 10 $L.min^{-1}$.

The NaF was used as a molecular chemical tracer according to European standard procedure on aerosol medical devices (NF EN 13544–1). The NaF concentration in the samples was assessed by conductimetry (PerfectION™ combined with a SevenGo pro™ F− electrode, Mettler Toledo, France). Finally, the MMAD and the geometric standard deviation (GSD) of the nebulised particles were calculated[31–34].

^{99m}Tc-DTPA was used as a molecular radiotracer. The deposited fraction on each DLPI stages was collected on an in-house impermeable plastic cover. The amount of ^{99m}Tc-DTPA was quantified using Packard Cobra II auto-gamma counting system (Perkin-Elmer, Waltham, MA, USA). Then, the activity median aerodynamic diameter (AMAD) and the geometric standard deviation (GSD) of the nebulised particles were calculated.

Finally, the SRP was used as a nanotracer. The nebuliser was filled with 3 mL of SRP suspension (corresponding to 900 µmol of SRP). After nebulisation, the deposited fraction on each DLPI stages was collected using 1 mL of deionised water. The amount of Gd was then quantified by ICP-MS (NexIon 2000, PerkinElmer, Wellesley, MA). Samples for ICP-MS were placed in polytetrafluoroethylene tube compatible with the microwave oven CEM Mars 5. Then, 10 mL of HNO3 69% was added. After cooling, the samples were diluted in HNO3 1% to reach a sample concentration of 1 g/L. Finally, the MMAD and the geometric standard deviation (GSD) of the nebulised particles were calculated. Further information is provided in the Supplementary Information.

Aerosol Output

The aerosol output delivered by the nebuliser (ie the emitted aerosol fraction) was assessed according to the NF EN 13544−1 European standard using a residual gravimetric method[31,35] Briefly, the nebuliser was activated with 3 mL of solution/suspension containing the studied tracers (NaF and SRP), until atomisation. The nebuliser is connected to 2 absolute electrostatic filters: one inhalation filter which is connected to a respiratory pump (PARI Compas II, PARI GmbH, 500 mL tidal volume with sinusoidal pattern; 15 cycles/min; I/E of 1:1) and one expiratory filter placed after a one-way valve. The mass of tracer was measured on the filters before and after nebulisation. Results are presented as a proportion of the tracer in the inhalable filter versus the initial quantity of tracer introduced in the nebuliser.

Regional Aerosol Deposition Assessed by Gamma-Camera Imaging

Nebulised radionuclides used for scintigraphy imaging were ^{99m}Tc-DTPA as molecular radiotracer and ^{111}indium chloride (^{111}In) chelated on the SRP as a nanoparticulate radiotracer (^{111}In-SRP). The nebulisation was performed with 100 MBq/3 mL of ^{99m}Tc-DTPA and 60 MBq/3 mL of ^{111}In-SRP suspension. The chelation of ^{111}In on SRP was performed following the protocol developed by Morlieras et al[36] and modified for the purification process. Briefly, the nanoparticles were suspended in milliQ water at the concentration of 100 mg/mL. Then, the SRP suspension was mixed with ^{111}In (ratio 1:2). Citrate buffer (pH 5; 100mM) was added qs for 10 mL. The mixture was incubated at 50°C under stirring for 15 minutes. Purification was achieved with Vivacon® centrifuge filter 2kDA MWCO (Sartorius, Göttingen, Germany). The complete process of the SRP radiolabelling with ^{111}In could be found in the Supplementary Information. The nebuliser was connected to the ENT by a mouthpiece, sealing was conducted to avoid any loss of generated aerosol. To avoid exposure due to exhaled aerosol, an expiratory filter was positioned after a one-way valve.

The gamma-camera imaging was realized as previously described[24,26] 2D scintigraphies were conducted on three respiratory tracts for each type of tracer with a variable angle dual detector Single Photon Emission Computed Tomography/Computed Tomography (SPECT-CT, SYMBIA T2; Siemens, Knoxville, TN). The initial radioactive dose in the nebuliser was calculated from the difference of activity between the full and empty syringe. After inhalation of the aerosol, each component of the system was imaged with 3-min anterior/posterior exposition: nebuliser (with dead volume), expiratory filter, ENT replica and respiratory tract. Further information is given in Supplementary Information.

Regional Aerosol Deposition Assessed by MRI

MRI contrast agents used were gadoterate meglumine (Clariscan® Gé, GE Healthcare) as a molecular tracer and SRP as nanoparticulate (NP) tracer. The chosen concentration of each tracer was equivalent to 300 mM of gadolinium.

The protocol allowing the imaging of nebulised SRP in isolated porcine lungs was previously described.[30] Acquisitions were performed with a 3 Tesla whole body magnet (Vantage Galan 3T ZGO, Canon Medical Systems Corporation, Japan) using a T_1-weighted 3D UTE (Ultra short Echo Time) MRI sequence. Detailed information about the imaging protocol are available in the Supplementary Information and in the paper from Crémillieux et al.[30]

Signal enhancement was defined as:

$$\frac{SNR_{aerosol} - SNR_{baseline}}{SNR_{baseline}}$$

where $SNR_{aerosol}$ and $SNR_{baseline}$ correspond to the signal-to-noise ratio (SNR) measured after and before nebulisation of the tracer, respectively. Then, the T_1 value was used to estimate the concentration, C (mM), of Gd^{3+} ion in the lungs as follows:[37]

$$C = \frac{1}{r_1}\left(\frac{1}{T_{1post}} - \frac{1}{T_{1pre}}\right)$$

where $T1_{pre}$ and $T1_{post}$ are the longitudinal relaxation times before and after nebulisation of the tracer and r_1 is the longitudinal relaxivity induced by gadolinium ion. The measurements of SNR values in the region of interest (ROI) and the generation of maximum intensity of projection (MIP) were performed using OsiriX (Geneva, Switzerland). The computing of T_1 values was realized using open-source SciLab software (ESI, Paris, France). Further information is provided in the Supplementary Information.

Lastly, samples of lung parenchyma (two pieces of 1.5 g each per lobe for each tracer) were used to quantify gadolinium concentration using ICP-MS (NexIon 2000, PerkinElmer, Wellesley, MA, USA). Following sampling, the pieces were placed in a PTFE tube compatible with the microwave oven CEM Mars 5 in 10 mL of HNO_3 69%. After cooling, the samples were diluted in HNO_3 1% to reach a concentration of tissue of 1 g/L.

Statistical Analyses

Statistical analyses were performed using GraphPad Prism 8 (GraphPad Software Inc., San Diego, CA, USA). For the aerosol size and output determination, a one-way ANOVA with Tukey's *post hoc* multiple comparison test was performed. For the quantitative assessment of regional radioaerosol deposition in the ex vivo model, a two-way ANOVA with Sidak's *post hoc* multiple comparison test was used. For MRI quantitative assessment, multiple t-tests were used and p-values were adjusted with Holm-Sidak's method.

For all tests, significance was fixed at 5%. The data are presented as mean value ± standard deviation (SD).

Results

Aerosol Features of the Tracers

Features of nebulised tracers are presented in Table 1. No statistical difference was observed for the MMAD of the aerosol or for the output, whatever tracer used. Indeed, the aerosols containing ^{99m}Tc-DTPA or SRP tracers (3.40 ± 0.15 µm vs. 3.60 ± 0.05 µm; p=0.1373) and the aerosols containing the molecular tracers NaF or ^{99m}Tc-DTPA (3.65 ± 0.10 µm vs. 3.40 ± 0.15 µm; p=0.0668) presented similar MMAD around 3.5 µm.

Regional Aerosol Deposition Assessed by Gamma-Camera Imaging

The regional aerosol deposition of both molecular and nanoparticulate tracers were assessed by planar scintigraphies using gamma camera (n=3 for each tracer). Figure 1 shows planar scintigraphies obtained with ^{99m}Tc-DTPA and ^{111}In-SRP. As seen, there is no qualitative difference in term of aerosol deposition pattern, whatever the tracer used. Indeed, these scintigraphies show a highly homogeneous lung deposition of aerosol. Quantification of the deposited fractions within the ex vivo model was performed. Results are presented in Table 2 as proportion ± standard deviation (SD) of the nominal dose of radioactivity (ie the initial activity injected in the nebuliser tank). According to the nebulised activity, for both tracers, there is no significant difference (54 ± 2% vs 52 ± 3%; p=0.9285). Besides, significant differences were noticed between the deposited fractions: a higher exhaled fraction, and a 2-fold lower ENT deposition (14 ± 3% vs 22 ± 1%; p=0.0207) and lung deposition (9 ± 3% vs 21 ± 6%; p=0.0022) is observed for the nanoparticulate tracer compared to the molecular tracer. However, despite this disparate dose of tracers reaching the ENT or lung regions, the regional aerosol deposition profile remains similar with approximately 50% of the deposited fraction in the lungs whatever the tracers (ENT region: 51 ± 6% for ^{99m} Tc-DTPA vs 62 ± 12% for ^{111}In-SRP; lung region: 49 ± 6% for ^{99m},Tc-DTPA vs 38 ± 12% for ^{111}In-SRP; p=0.2426).

Ex vivo Regional Deposition Assessed by MRI

Signal enhancement in the lung after nebulisation is presented in Figure 2. Here, the lungs received two consecutive nebulisation of 6 mL of SRP suspension for a cumulative amount of Gd^{3+} nebulised of 3.6 mmol (1.8 mmol of Gd^{3+}/nebulisation).

A large increase of the image signal intensity can be noticed from the two exemplary coronal images (excitation flip angle of 25°) acquired before and after the nebulisation of the nanoparticles. This signal intensity increase is consistent with the lowering of T_1 values due to the presence of gadolinium ion in the lungs. As seen from the image, this SE was homogenous in the lungs, including its most distal regions. Some anatomical information accessible following the nebulisation of the aerosol and the resulting increase in SNR and contrast are highlighted in this MRI image with a red arrow and a yellow arrow pointing, respectively, a lung fissure separating two lobes and the mosaic-like pattern of the secondary pulmonary lobules enclosed by the hypo-intense interlobular septum. In the absence of aerosol, these anatomical structures are not observable in the MRI images.

To preferentially visualize the airways, a 3D MIP was applied to a 3D acquisition, shown in Figure 3. Up to eight generations of airways are visible from the trachea to the bronchi of the secondary lobules with a diameter of a few millimetres, close to the ultimate spatial resolution of the image. As Figure 2, this image was obtained after two consecutive nebulisation of SRP suspension. Before nebulisation, this level of anatomical detail was not present on the MRI images.

Similar qualitative and quantitative results were observed when nebulizing in the lung an aerosol of gadoterate meglumine (Gd-DOTA) solution. For the same amount of nebulised gadolinium (*ie* 3.6 mmol), the signal enhancements obtained with an excitation flip angle of 25° were equal to 171% and 208% for the SRP and the Gd-DOTA, respectively.

The concentrations of Gd^{3+} ion, derived from the measured longitudinal relaxation times T_1 after nebulisation, were found equal to 1029 ± 22 µM for SRP and 1957 ± 179 µM for Gd-DOTA.

The amounts of gadolinium measured in the lung samples with ICP-MS were 40 ± 9.1 µg/g and 78.6 ± 10.5 µg/g for the SRP and Gd-DOTA, respectively. By approximating the tissue density at 1 kg/L, these quantities correspond to a Gd^{3+} concentration of 0.25 mM and 0.5 mM in the tissue samples following SRP and Gd-DOTA nebulisation, respectively.

Discussion

The regional aerosol deposition was recorded by planar scintigraphies for each radiotracer. The quantitative assessment of deposited fractions was conducted for each component of the ex vivo model. The results presented in Table 2 show that there was no significant difference in the nebulised

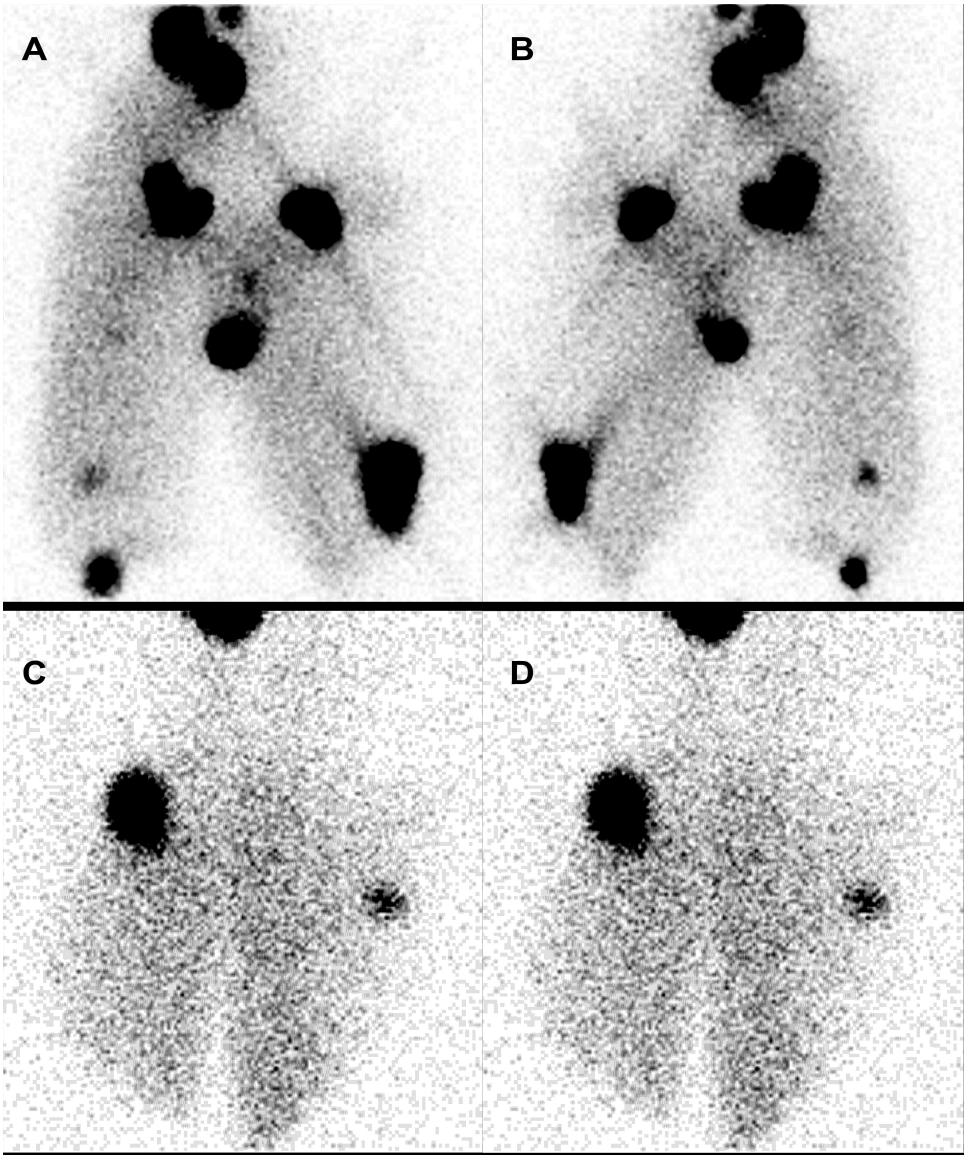

Figure 1 Planar scintigraphic images of regional aerosol deposition in the ex vivo model. (**A, B**) images obtained with ^{99m}Tc-DTPA molecular tracer, respectively anterior and posterior views. (**C, D**) images obtained with ^{111}In-SRP nanoparticulate tracer, respectively anterior and posterior views. Hotspots correspond to wounded and sutured region of the respiratory tracts.

activity of the aerosol, meaning that the nebulisation performances are not changed when a nanoparticulate suspension was used compared to a molecular tracer. These results are perfectly in accordance with the similar output rate observed in vitro for these two tracers (Table 1). However, the deposited fractions showed discrepancies. Significant differences were found between the two tracers, with 3-fold higher exhaled fraction and 2-fold lower ENT and respiratory tract fractions for the ^{111}In-SRP by comparing with ^{99m}Tc-DTPA. Nonetheless, the aerosol regional deposition profile remains similar (with approximately 50% of the radioaerosol deposited in the lung and the ENT region). Besides, as shown in Figure 1, despite the lower deposition of ^{111}In-SRP aerosol in the respiratory tract, the amount of radioaerosol is sufficient to allow quantitative imaging. Moreover, the deposition pattern of ^{111}In-SRP is as homogeneous as the one obtained with the molecular tracer.

As easily seen, the scintigraphic images on Figure 1 present hotspots. These hyperfixations of the radioaerosol are due to the inevitable cuts present on the lungs. Despite being thoroughly sutured, these wounds of the lung parenchyma created regions with decreased resistances of the airflow and, thus, representing a preferred way for the airflow. However, this particular point does not represent an impairment to assess the homogeneity of the deposited aerosol as previously discussed.[26] Overall, these

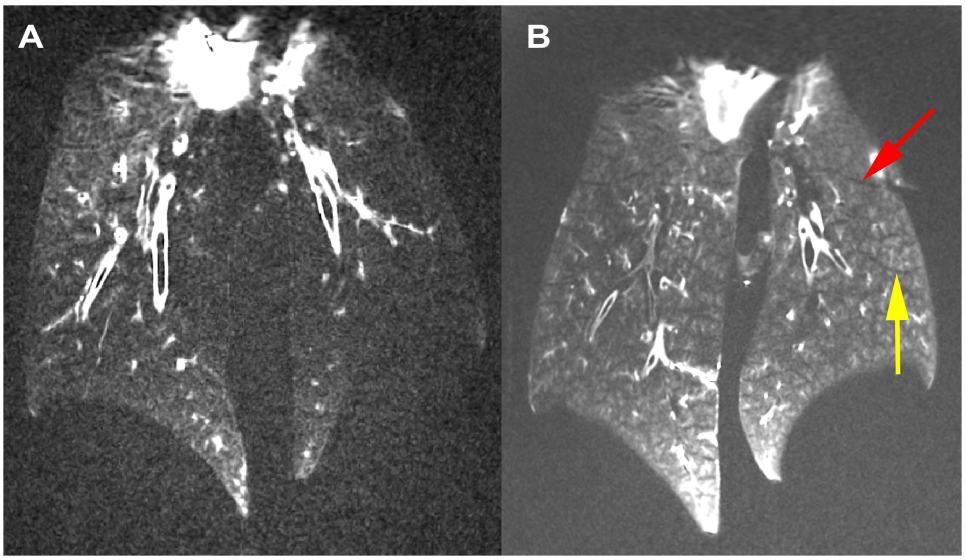

Figure 2 (**A**) Coronal slice extracted from a 3D dataset obtained before nebulisation. (**B**) Coronal slice extracted from a 3D dataset obtained after nebulisation of 12 mL of nanoparticle suspension (3.6 mmol of Gd^{3+}) in both lungs. The red arrow is pointing a lung fissure separating two lobes and the yellow arrow is pointing the secondary pulmonary lobules (mosaic pattern) visible following the nebulisation of nanoparticles.

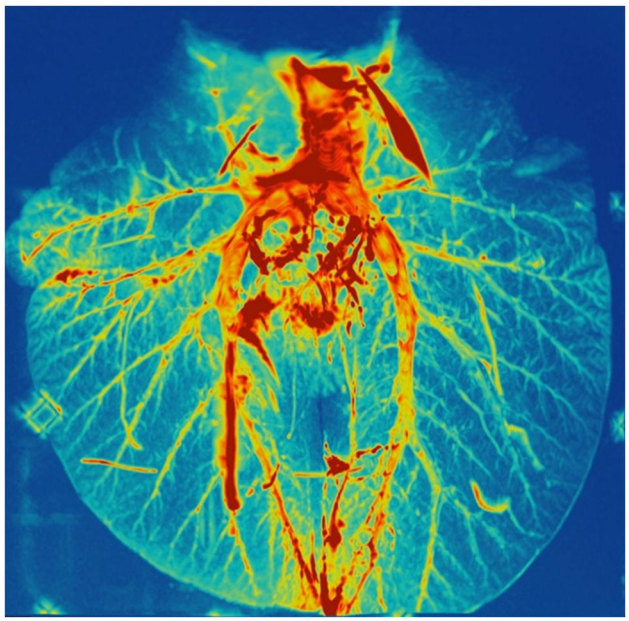

Figure 3 3D maximum intensity projection (MIP) image obtained after nebulisation of 12 mL of nanoparticles suspension (3.6 mmol of Gd^{3+}). Small bronchi, down to the 8th generation of the respiratory tract could be visualized.

experiments supported that it is feasible to use a conventional clinical nebuliser to aerosolise SRP suspension. Furthermore, the nebulisation performances are similar to a conventional molecular solution. Nevertheless, discrepancies were observed in the nebulisation process between the molecular and the nanoparticulate tracer. These discrepancies could be explained by the differences in the physicochemical properties of the nebulisation media for the molecular and nanoparticulate tracers. Particularly, the modification of the composition, and thus, the viscosity could have a major impact on the behaviour of aerosolised droplets over time. Further experiments would be needed to thoroughly assess this point.

MR images obtained after nebulisation of SRP and Gd-DOTA aerosols showed a homogeneous and complete enhancement of the pulmonary parenchyma indicating that the aerosol penetrates deep into the lung to the level of bronchioles whom diameter is smaller than the dimension of the voxel (1 mm^3). For the same amount of nebulised gadolinium, a 2-fold higher concentration of Gd^{3+} ion is measured in the lungs for Gd-DOTA than SRP. This MRI-based result is coherent with ICP-MS: twice as much gadolinium for Gd-DOTA. These results are consistent with the scintigraphic measurements indicating that 21% of the radioactive dose was deposited in the lungs with ^{99m}Tc-DTPA as compared to 9% of the radioactive dose with the ^{111}In-SRP.

The difference observed between the Gd^{3+} concentration obtained using MRI (1 mM and 1.96 mM) and ICP-MS (0.25 mM and 0.5 mM) after nebulisation of SRP and Gd-DOTA could be explained by the intrinsic difference in the way each of these techniques measure gadolinium concentration. The ICP-MS measurement provides an average concentration in the tissue sample and does not contain information on the distribution of the gadolinium

Table 1 Aerosol Characteristics After Nebulization for the Nanoparticular Tracer (SRP) and the Molecular Tracers (NaF and ^{99m}Tc-DTPA): Mass Median Aerodynamic Diameter (MMAD) and Geometric Standard Deviation (GSD) Calculated Using DLPI Results. The Aerosol Output is Expressed as a Proportion of the Tracer Initially Introduced into the Nebulizer Tank. N/A: Not Available

Tracer	MMAD (μm)	GSD	Aerosol Output (%)
NaF	3.65 ± 0.10	2.55 ± 0.05	26.5 ± 3.0
^{99m}Tc-DTPA	3.40 ± 0.15	2.70 ± 0.05	N/A
SRP	3.60 ± 0.05	2.35 ± 0.10	29.3 ± 1.0

within the sample. Contrarily, the MRI measurement is sensitive to the heterogeneities in the distribution of gadolinium, even at a sub-pixel level. In the case of the lungs, the MRI signal intensity from Gd-free lung parenchyma regions is very weak, close to the noise level, and has little contribution to the overall MRI signal. As a result, the MRI signal originates mainly from regions where gadolinium is present and concentrated.

It is very likely that after deposition, the Gd-based nanoparticles and molecular contrast agents remain in the fluids that are lining the walls of the respiratory tract (from the bronchi down to the alveoli) and that there is no diffusion in the lung parenchyma. A simple calculation, considering standard pulmonary physiological parameters, allows to ensure the plausibility of this hypothesis. First, one can estimate the total lung capacity at 5 L, *ie* 2.5 L per lung. Assuming a lung tissue density of 0.35g/L, this is translated into a lung tissue volume of 1.35 L per lung. Based on the ICP-MS measurements, that gives 0.338 mmol and 0.675 mmol of Gd^{3+} deposited in one lung for SRP and Gd-DOTA, respectively. These values represent 9% and 19% of the nominal dose of 3.6 mmol Gd^{3+} for SRP and Gd-DOTA, respectively, which are close to the values obtained with the gamma-camera imaging and therefore indicative of the relevance of the calculation.

The concentrations of Gd^{3+} ions obtained by MRI are four times higher than those obtained by ICP-MS. They can be understood as the consequence of the distribution of aerosols in one quarter only of the lung tissue volume. Taking up our previous calculation, this volume would equal to a lung tissue volume of 0.34 L. Assuming that this compartment corresponds to the lining fluid in the respiratory tract, spread over a total surface area of 70 m2 per lung, one end up with a fluid thickness of 5 micrometres. Here again, this number is compatible with the non-physiological and ex vivo experimental conditions of the study and the probable presence of excess fluids in the airways.

In this study, two techniques were compared to precisely assess the regional deposition of aerosols in the respiratory tract. On the one hand, gamma-camera imaging is the gold standard method which allows a relatively easy assessment of the deposition pattern with an accurate semi-quantitative profile and potential metabolic following of the tracer. However, this method has some limitations, such as the spatial resolution and the follow-up of different radionuclides at the same time. Moreover, gamma-camera imaging exposes patients to ionizing radiation. Contrarily, the MRI is an upcoming technique with important recent improvements to image the lungs. This method has a very

Table 2 Deposited Fractions in Each Component of the ex vivo Respiratory Model. Data are Expressed as Mean ± Standard Deviation of the Nominal Dose of Radioactivity or of the Total Deposited Dose. Nebulized Activity Corresponds to the Proportion of Initial Radioactivity That Was Efficiently Nebulized

	Nebulized Activity in % of the Nominal Dose	Regional Aerosol Deposition Expressed in % of the Deposited Dose Within the Respiratory Tract (ENT and Lung Regions)		Regional Aerosol Deposition Expressed in % of the Nominal Dose Initially Introduced into the Nebulizer		
	Nebulized activity	ENT deposition	Lung deposition	Exhaled Fraction	ENT deposition	Lung deposition
^{99m}Tc-DTPA (molecular)	52 ± 3%	51 ± 6%	49 ± 6%	8 ± 3%	22 ± 1%	21 ± 6%
^{111}In-SRP (nanoparticles)	54 ± 2%	62 ± 12%	38 ± 12%	26 ± 4%	14 ± 3%	9 ± 3%

Abbreviations: Exhaled, expiratory filter = one-way valve; Interface, mouthpiece + sealing plasticine; ENT, 3D-printed head replica; Respiratory tracts, porcine respiratory tract + pump filter.

good spatial resolution and is completely unharming for patients. However, the quantification of the deposition with MRI necessitates a contrast agent with known T_1 relaxivity in the experimental conditions. Moreover, as MRI is based on the detection of the water, imaging the lungs, which exert a reduced tissue density, remains a challenge.

To image the SRP deposition with MRI, Bianchi et al[38] used a dedicated lung MRI protocol in healthy mice. They assessed the MRI signal variations in the lungs following the intratracheal administration (IT). They showed that MRI acquisitions can be used to quantitatively monitor the biodistribution and the pharmacokinetics of the nanoparticles in the lungs of freely breathing animals. The implementation of pharmacokinetic models in lungs allowed them to identify the elimination pathways and the elimination time constants of the nanoparticles. Considering the favourable kinetics of these nanoparticles in the lungs (residence time in the order of 1 hour in the lung tissue) followed by an effective and complete renal clearance, several animal models of lung disease were then investigated. For instance, Tassali et al[39] investigated the application of lung MRI protocol combined with the intratracheal administration of the SRP in a bleomycin-induced fibrotic mouse model. The authors reported an MRI signal enhancement of 120% in fibrotic lesions as compared to 50% in healthy tissues and a two-fold increase of contrast-to-noise ratio between fibrotic and healthy tissue. They also assessed their clearance and observed that elimination time constant was 54% higher in fibrotic lesions. The authors concluded that this passive targeting of fibrotic lesions might help to monitor the efficacy of antifibrotic drugs and therapeutic molecules targeting this disease. Similarly, these theranostic nanoparticles can be delivered passively to lung tumours. Bianchi et al[7] reported an original passive targeting of lung tumours in an orthotopic mouse model of lung cancer. Indeed, nanoparticles are retained in the tumour after administration through the airways but could translocate to blood circulation when deposited in healthy lungs. After the passage to blood circulation, they can also target tumours via Enhanced Permeability and Retention (EPR) effect. The authors evaluated two administration routes for these nanoparticles, IV and IT administration and found that the IT route was more effective for targeting and detecting the lung tumour. Moreover, following intrapulmonary administration of these radio-sensitizing nano-assemblies, the animals were exposed to radiotherapy and a 45%-increase of the mean survival time was reported.[40]

Despite these positive and promising preclinical results, the translation from small animals to humans of these diagnostic and therapeutic protocols using intrapulmonary administered nanoparticles remains challenging and requires further methodological validation steps on both the imaging and the delivery aspects. Indeed, there is an important gap between preclinical and clinical for pulmonary delivery of nanoparticles. One of the major pitfalls is the administration of the nanoparticles in the tracheobronchial tree. In small animal models, IT administrations are mainly performed by direct instillation through a specific needle placed in the trachea while the aerosolization is performed with a syringe containing a mixture of the nanoparticle suspension and air.[11,38–40] However, this mode of administration was proved to generate an uneven pattern of deposition of the aerosol which could generate impairment to human transposition.[41] Contrarily, inhalation of an aerosol generated by a nebuliser resulted in a homogeneous deposition and, thus, an easier extrapolation to human.[42] This difference of deposition pattern between instillation and inhalation is well documented in nanotoxicology[43–45] and was also found in mechanically ventilated patients.[46] Another major pitfall in animal-human transposition is the important difference in terms of the anatomy of the airways and the respiratory physiology between rodent models and human.[47–50] This limitation could be partially overcome by using bigger animal such as pigs or non-human primates however ethical restrictions are much stronger in this case. Therefore, other models such as ex vivo respiratory models appear to be an interesting preclinical tool to assess aerosol deposition in healthy and pathological-like respiratory tracts.[24,26] Composed a 3D-printed Ear-Nose-Throat (ENT) replica connected to a porcine respiratory tract (RT) in a sealed enclosure simulating passive ventilation, these models proved to be an innovative way to quantitatively assess aerosol deposition into the respiratory tract.[30,51] Hence, it could be easier to assess aerosol deposition into the lungs and then to transpose it to human.

Considering the advantages and the limitations of each technique, it appears that MRI could be an interesting surrogate for gamma-camera imaging due to the absence of ionizing radiation and, thus, allowing multiplication of the acquisitions on the same patients. However, further improvements in the quantification technique based on MRI imaging need to be addressed. One of the major drawbacks being the need for important preliminary characterization of the contrast agent. Lastly, an interesting

way of research could be the development of co-assessment of aerosol deposition in the RT trough the combination of gamma-camera imaging and MRI. Therefore, TEP-MRI technique could be a promising tool for such studies, especially as SRP – radiolabelled with ^{68}Gallium – has shown interesting properties for PET/MRI.[52]

Conclusion

Through this study, two main aims were hypothesized. First, the feasibility to aerosolize nanoparticles with a clinically used nebuliser with the same properties as a molecular tracer. This was proved to be validated by the measurement of the MMAD and the aerosol output, which were statistically equivalent. Second, we speculated that the two aerosols, molecular and nanoparticulate, would have similar regional deposition pattern on an ex vivo respiratory model. To confirm this point, we used a multimodal approach by using scintigraphy and MRI acquisition to qualitatively and quantitatively assess the deposited aerosol in the model. With both techniques, we observed a homogenous pattern of deposition with the SRP aerosol, pattern which is like the one obtained with a molecular tracer. The quantitative assessment of the deposition showed a 2-fold lower quantity of aerosol deposited into the respiratory tract with the SRP aerosol than the molecular tracer aerosol, for both imaging techniques. Thus, the consistency of the generated results seemed to validate our hypotheses.

Despite the limitations of the ex vivo model used to assess the regional deposition pattern of the aerosol, we proved that the aerosolization of a nanoparticulate suspension could be achieved with a clinical nebuliser. Therefore, we hope that these promising preclinical findings could facilitate the transfer of the aerosolized SRP to the clinic.

Acknowledgments

The authors are grateful to Canon Medical Systems for their technical and scientific support regarding MRI studies.

Funding

The aerosol size and output determination and the scintigraphic assessment of the regional aerosol deposition were funded by the French Agency for Research [ANR-17-CE19-0002-01]. The MRI studies were carried out within the IBIO (Institut de Bio-Imagerie de Bordeaux) and were achieved within the context of the Laboratory of Excellence TRAIL ANR-10-LABX-57. NH TherAGuIX® supported the cost of radionuclides for the radiolabelling of the AGuIX® nanoparticles with 111In.

Disclosure

FL and OT must disclose the patent WO2011/135101. FL, OT and YC must disclose the patent WO2013153197. These patents protect the AGuIX® nanoparticles described in this publication and their administration via the airways. FL, OT and YC are employees from NH TherAGuIX® that is developing the AGuIX® Nanoparticles. FL and OT possess shares of this company. OT reports grants, personal fees from NH TherAguix, during the conduct of the study; In addition, OT has a patent WO200550302 licensed. FL reports grants, personal fees from Nh TherAguix, during the conduct of the study and outside the submitted work. YC reports personal fees from NH TherAguix, outside the submitted work. The aforementioned authors report no other potential conflicts of interest in this work. The other authors report no conflicts of interest in this work.

References

1. Lux F, Tran VL, Thomas E, et al. AGuIX® from bench to bedside—Transfer of an ultrasmall theranostic gadolinium-based nanoparticle to clinical medicine. *Br J Radiol*. 2018;92(1093):20180365. doi:10.1259/bjr.20180365
2. Verry C, Sancey L, Dufort S, et al. Treatment of multiple brain metastases using gadolinium nanoparticles and radiotherapy: NANO-RAD, a Phase I study protocol. *BMJ Open*. 2019;9(2): e023591. doi:10.1136/bmjopen-2018-023591
3. Bort G, Lux F, Dufort S, Crémillieux Y, Verry C, Tillement O. EPR-mediated tumor targeting using ultrasmall-hybrid nanoparticles: from animal to human with theranostic AGuIX nanoparticles. *Theranostics*. 2020;10(3):1319-31.
4. Sancey L, Lux F, Kotb S, et al. The use of theranostic gadolinium-based nanoprobes to improve radiotherapy efficacy. *Br J Radiol*. 2014;87(1041):20140134.
5. Lux F, Mignot A, Mowat P, et al. Ultrasmall rigid particles as multimodal probes for medical applications. *Angew Chem Int Ed*. 2011;50 (51):12299-303.
6. Mignot A, Truillet C, Lux F, et al. A top-down synthesis route to ultrasmall multifunctional gd-based silica nanoparticles for theranostic applications. *Chem – Eur J*. 2013;19(19):6122-36.
7. Bianchi A, Dufort S, Lux F, et al. Targeting and in vivo imaging of non-small–cell lung cancer using nebulised multimodal contrast agents. *Proc Natl Acad Sci*. 2014;111(25):9247-52.
8. Kryza D, Taleb J, Janier M, et al. Biodistribution study of nanometric hybrid gadolinium oxide particles as a multimodal SPECT/MR/optical imaging and theragnostic agent. *Bioconjug Chem*. 2011;22(6):1145-52.
9. Miladi I, Duc GL, Kryza D, et al. Biodistribution of ultra small gadolinium-based nanoparticles as theranostic agent: application to brain tumors. *J Biomater Appl*. 2013;28(3):385-94.
10. Miot-Noirault E, Vidal A, Morlieras J, et al. Small rigid platforms functionalization with quaternary ammonium: targeting extracellular matrix of chondrosarcoma. *Nanomedicine Nanotechnol Biol Med*. 2014;10(8):1887-95.

11. Bianchi A, Lux F, Tillement O, Crémillieux Y. Contrast enhanced lung MRI in mice using ultra-short echo time radial imaging and intratracheally administrated Gd-DOTA-based nanoparticles. *Magn Reson Med*. 2013;70(5):1419-26. doi:10.1002/mrm.24580
12. Paranjpe M, Müller-Goymann CC. Nanoparticle-mediated pulmonary drug delivery: a review. *Int J Mol Sci*. 2014;15(4):5852-73.
13. Beck-Broichsitter M, Knuedeler M-C, Oesterheld N, Seeger W, Schmehl T. Boosting the aerodynamic properties of vibrating-mesh nebulised polymeric nanosuspensions. *Int J Pharm*. 2014;459 (1-2):23-9. doi:10.1016/j.ijpharm.2013.11.040
14. Beck-Broichsitter M, Kleimann P, Schmehl T, et al. Impact of lyoprotectants for the stabilization of biodegradable nanoparticles on the performance of air-jet, ultrasonic, and vibrating-mesh nebulisers. *Eur J Pharm Biopharm Off J Arbeitsgemeinschaft Pharm Verfahrenstechnik EV*. 2012;82(2):272-80.
15. Gaspar MM, Gobbo O, Ehrhardt C. Generation of liposome aerosols with the Aeroneb Pro and the AeroProbe nebulisers. *J Liposome Res*. 2010;20(1):55-61.
16. Bridges PA, Taylor KM. An investigation of some of the factors influencing the jet nebulisation of liposomes. *Int J Pharm*. 2000;204(1-2):69-79. doi:10.1016/S0378-5173(00)00477-4
17. Dailey LA, Schmehl T, Gessler T, et al. Nebulisation of biodegradable nanoparticles: impact of nebuliser technology and nanoparticle characteristics on aerosol features. *J Control Release off J Control Release Soc*. 2003;86(1):131-44.
18. Beck-Broichsitter M, Knuedeler M-C, Schmehl T, Seeger W. Following the concentration of polymeric nanoparticles during nebulisation. *Pharm Res*. 2013;30(1):16-24.
19. Elhissi AMA, Faizi M, Naji WF, Gill HS, Taylor KMG. Physical stability and aerosol properties of liposomes delivered using an air-jet nebuliser and a novel micropump device with large mesh apertures. *Int J Pharm*. 2007;334(1-2):62-70. doi:10.1016/j.ijpharm.2006.10.022
20. Anton N, Jakhmola A, Vandamme TF. Trojan microparticles for drug delivery. *Pharmaceutics*. 2012;4(1):1-25.
21. Tsapis N, Bennett D, Jackson B, Weitz DA, Edwards DA. Trojan particles: large porous carriers of nanoparticles for drug delivery. *Proc Natl Acad Sci U S A*. 2002;99(19):12001-5.
22. Mangal S, Gao W, Li T, Zhou QT. Pulmonary delivery of nanoparticle chemotherapy for the treatment of lung cancers: challenges and opportunities. *Acta Pharmacol Sin*. 2017;38(6):782-97.
23. Li X, Anton N, Ta TMC, Zhao M, Messaddeq N, Vandamme TF. Microencapsulation of nanoemulsions: novel Trojan particles for bioactive lipid molecule delivery. *Int J Nanomedicine*. 2011;6:1313-25.
24. Perinel S, Leclerc L, Prévôt N, et al. Micron-sized and submicron-sized aerosol deposition in a new ex vivo preclinical model. *Respir Res*. 2016;17(1). doi:10.1186/s12931-016-0395-7
25. Perinel S, Pourchez J, Leclerc L, et al. Development of an ex vivo human-porcine respiratory model for preclinical studies. *Sci Rep*. 2017;7(1). doi:10.1038/srep43121
26. Montigaud Y, Perinel-Ragey S, Plantier L, et al. Development of an ex vivo preclinical respiratory model of idiopathic pulmonary fibrosis for aerosol regional studies. *Sci Rep*. 2019;9(1):1-11.
27. Perinel S, Forest V, Landraud M, et al. Deposition pattern of aerosolized Legionella using an ex vivo human-porcine respiratory model. *Int J Hyg Environ Health*. 2018;221(2):252-9.
28. Ragey SP, Pourchez J, Leclerc L, et al. A human-like ex vivo preclinical model for aerosol deposition studies. *Eur Respir J*. 2015;46 (suppl 59):PA3581.
29. West JB, West JB. *Pulmonary Pathophysiology: The Essentials*. 8th ed. Philadelphia: Wolters Kluwer/Lippincott Williams & Wilkins Health; 2012:183.
30. Crémillieux Y, Montigaud Y, Bal C, et al. Three-dimensional quantitative MRI of aerosolized gadolinium-based nanoparticles and contrast agents in isolated ventilated porcine lungs. *Magn Reson Med*. 2020;83(5):1774-82.
31. Leclerc L, Pourchez J, Aubert G, et al. Impact of airborne particle size, acoustic airflow and breathing pattern on delivery of nebulised antibiotic into the maxillary sinuses using a realistic human nasal replica. *Pharm Res*. 2014;31(9):2335-43.
32. Leclerc L, Merhie AE, Navarro L, Prévôt N, Durand M, Pourchez J. Impact of acoustic airflow on intrasinus drug deposition: new insights into the vibrating mode and the optimal acoustic frequency to enhance the delivery of nebulised antibiotic. *Int J Pharm*. 2015;494 (1):227-34.
33. El Merhie A, Navarro L, Delavenne X, Leclerc L, Pourchez J. A new strategy to improve drug delivery to the maxillary sinuses: the frequency sweep acoustic airflow. *Pharm Res*. 2016;33(5):1074-84.
34. Moghadam SJ, Navarro L, Leclerc L, Hodin S, Pourchez J. Toward smart Nebulisation: engineering acoustic airflow to penetrate maxillary sinuses in chronic rhinosinusitis. *Int J Pharm*. 2018;546 (1):188-93.
35. Vecellio None L, Grimbert D, Bordenave J, et al. Residual gravimetric method to measure nebuliser output. *J Aerosol Med*. 2004;17 (1):63-71.
36. Morlieras J, Chezal J-M, Miot-Noirault E, et al. In vivo evidence of the targeting of cartilaginous tissue by pyridinium functionalized nanoparticles. *Chem Commun*. 2013;49(29):3046-8.
37. Martin AR, Thompson RB, Finlay WH. MRI measurement of regional lung deposition in mice exposed nose-only to nebulised superparamagnetic iron oxide nanoparticles. *J Aerosol Med Pulm Drug Deliv*. 2008;21(4):335-42.
38. Bianchi A, Dufort S, Lux F, et al. Quantitative biodistribution and pharmacokinetics of multimodal gadolinium-based nanoparticles for lungs using ultrashort TE MRI. *Magn Reson Mater Phys Biol Med*. 2014;27(4):303-16.
39. Tassali N, Bianchi A, Lux F, et al. MR imaging, targeting and characterization of pulmonary fibrosis using intra-tracheal administration of gadolinium-based nanoparticles. *Contrast Media Mol Imaging*. 2016;11(5):396-404.
40. Dufort S, Bianchi A, Henry M, et al. Nebulised gadolinium-based nanoparticles: a theranostic approach for lung tumor imaging and radiosensitization. *Small*. 2015;11(2):215-21.
41. Yang L, Gradl R, Dierolf M, et al. Multimodal precision imaging of pulmonary nanoparticle delivery in mice: dynamics of application, spatial distribution, and dosimetry. *Small*. 2019;15(49):1904112.
42. Yang L, Feuchtinger A, Möller W, et al. Three-dimensional quantitative co-mapping of pulmonary morphology and nanoparticle distribution with cellular resolution in nondissected murine lungs. *ACS Nano*. 2019;13(2):1029-41.
43. Oberdörster G, Cox C, Gelein R. Intratracheal instillation versus intratracheal inhalation of tracer particles for measuring lung clearance function. *Exp Lung Res*. 1997;23(1):17-34.
44. Shinohara N, Nakazato T, Tamura M, et al. Clearance Kinetics of Fullerene C60 nanoparticles from rat lungs after intratracheal C60 instillation and inhalation C60 exposure. *Toxicol Sci*. 2010;118 (2):564-73.
45. Landsiedel R, Sauer UG, Ma-Hock L, Schnekenburger J, Wiemann M. Pulmonary toxicity of nanomaterials: a critical comparison of published in vitro assays and in vivo inhalation or instillation studies. *Nanomed*. 2014;9(16):2557-85.
46. Klockare M, Dufva A, Danielsson A-M, et al. Comparison between direct humidification and nebulisation of the respiratory tract at mechanical ventilation: distribution of saline solution studied by gamma camera. *J Clin Nurs*. 2006;15(3):301-7.
47. Kuempel ED, Tran CL, Castranova V, Bailer AJ. Lung dosimetry and risk assessment of nanoparticles: evaluating and extending current models in rats and humans. *Inhal Toxicol*. 2006;18(10):717-24.
48. Sjaastad OV, Hove K, Sand O. Physiology of domestic animals. *Scan Vet Press*. 2010;808.
49. Reece WO. *Dukes' Physiology of Domestic Animals*. John Wiley & Sons; 2015:760.

50. Parent RA. *Comparative Biology of the Normal Lung*. Academic Press; 2015:835.
51. Montigaud Y, Georges Q, Pourchez J, et al. Aerosol delivery during invasive mechanical ventilation: development of a preclinical ex vivo respiratory model for aerosol regional deposition. *Sci Rep*. 2019;9 (1):17930.
52. Bouziotis P, Stellas D, Thomas E, et al. 68Ga-radiolabeled AGuIX nanoparticles as dual-modality imaging agents for PET/MRI-guided radiation therapy. *Nanomed*. 2017;12(13):1561-74.